JPn Neuroscience
The Journal of Physiology
J Physiol 591.10 (2013) pp 2563–2578

Cellular effects of acute direct current stimulation: somatic and synaptic terminal effects

Asif Rahman[1], Davide Reato[1], Mattia Arlotti[2], Fernando Gasca[3], Abhishek Datta[4], Lucas C. Parra[1] and Marom Bikson[1]

[1]*Department of Biomedical Engineering, The City College of New York (CCNY), The City University of New York (CUNY), USA*
[2]*Department of Electronics, Computer Science and Systems, University of Bologna, Cesena, Italy*
[3]*Institute for Robotics and Cognitive Systems and the Graduate School for Computing in Medicine and Life Sciences, University of Lübeck, Germany*
[4]*Laboratory of Neuromodulation, Spaulding Rehabilitation Hospital, Harvard Medical School, Boston, MA*

Key points

- The diversity of cellular targets of direct current stimulation (DCS), including somas, dendrites and axon terminals, determine the modulation of synaptic efficacy.
- Axon terminals of cortical pyramidal neurons are two–three times more susceptible to polarization than somas.
- DCS in humans results in current flow dominantly parallel to the cortical surface, which in animal models of cortical stimulation results in synaptic pathway-specific modulation of neuronal excitability.
- These results suggest that somatic polarization together with axon terminal polarization may be important for synaptic pathway-specific modulation of DCS, which underlies modulation of neuronal excitability during transcranial DCS.

Abstract Transcranial direct current stimulation (tDCS) is a non-invasive brain stimulation technique to modulate cortical excitability. Although increased/decreased excitability under the anode/cathode electrode is nominally associated with membrane depolarization/hyperpolarization, which cellular compartments (somas, dendrites, axons and their terminals) mediate changes in cortical excitability remains unaddressed. Here we consider the acute effects of DCS on excitatory synaptic efficacy. Using multi-scale computational models and rat cortical brain slices, we show the following. (1) Typical tDCS montages produce predominantly tangential (relative to the cortical surface) direction currents (4–12 times radial direction currents), even directly under electrodes. (2) Radial current flow (parallel to the somatodendritic axis) modulates synaptic efficacy consistent with somatic polarization, with depolarization facilitating synaptic efficacy. (3) Tangential current flow (perpendicular to the somatodendritic axis) modulates synaptic efficacy acutely (during stimulation) in an afferent pathway-specific manner that is consistent with terminal polarization, with hyperpolarization facilitating synaptic efficacy. (4) Maximal polarization during uniform DCS is expected at distal (the branch length is more than three times the membrane length constant) synaptic terminals, independent of and two–three times more susceptible than pyramidal neuron somas. We conclude that during acute DCS the cellular targets responsible for modulation of synaptic efficacy are concurrently somata and axon terminals, with the direction of cortical current flow determining the relative influence.

DOI: 10.1113/jphysiol.2012.247171

(Received 22 October 2012; accepted after revision 6 March 2013; first published online 11 March 2013)
Corresponding author A. Rahman: Department of Biomedical Engineering, The City College of The City University of New York, Convent Avenue at 140th Street, Steinman Hall, 4th Floor, T-454, New York, NY 10031, USA. Email: asiftr@gmail.com

Abbreviations ACSF, artificial cerebrospinal fluid; DCS, direct current stimulation; EF, electric field; FE, finite element; FEM, finite element model; fEPSP, field EPSP; HD-tDCS, high-definition transcranial direct current stimulation; MRI, magnetic resonance imaging; tDCS, transcranial direct current stimulation.

Introduction

Transcranial direct current stimulation (tDCS) is investigated as a non-invasive therapeutic tool to induce changes in neural excitability, but the cellular targets of stimulation remain unclear. During tDCS, current flow (∼1 mA) from an anode to a cathode electrode generates weak electric fields (EFs; $<1\,V\,m^{-1}$) across the cortex (Datta *et al.* 2009; Salvador *et al.* 2010). tDCS modulates cortical excitability in the primary motor cortex (Nitsche & Paulus, 2000, 2001; Antal *et al.* 2004), with anodal stimulation enhancing and cathodal stimulation diminishing corticospinal excitability, as measured by motor-evoked potentials elicited by transcranial magnetic stimulation (Nitsche *et al.* 2005). Similarly, in animal models of DCS, spontaneous and evoked cortical potentials were acutely facilitated under the anode and inhibited under the cathode (Creutzfeldt *et al.* 1962; Bindman *et al.* 1964; Purpura & McMurtry, 1965). The acute changes in synaptic efficacy by DCS may translate to enduring effects (short- or long-term plasticity) lasting over 1 h after stimulation, dependent on the duration of stimulation (typically minutes; Bindman *et al.* 1964; Gartside, 1968) and the nature of ongoing (synaptic) activity (Fritsch *et al.* 2010; Ranieri *et al.* 2012). Additionally, the acute effects of DCS are not homogeneous as the cellular effects of stimulation depend on neuronal morphology, stimulation intensity, neuronal orientation relative to the induced EF, and on the nature of the spontaneous/evoked activity (Chan & Nicholson, 1986; Tranchina & Nicholson, 1986; Chan *et al.* 1988; Andreasen & Nedergaard, 1996; Bikson *et al.* 2004; Joucla & Yvert, 2009; Radman *et al.* 2009). Here, we consider if characterizing the cellular targets of DCS may help reconcile acute neuromodulation patterns in a single framework. We specifically focus on the role of acute cortical DCS on presynaptic (afferent axon) *versus* postsynaptic (soma/dendrites) cellular compartments in modulating synaptic efficacy (Jefferys, 1981; Bikson *et al.* 2004; Fritsch *et al.* 2010; Kabakov *et al.* 2012; Ranieri *et al.* 2012).

Neuronal excitability in resting neurons is modulated by subthreshold DCS through cell membrane polarization (<1 mV polarization per $V\,m^{-1}$; Radman *et al.* 2009). While the increase in excitability under the anode is attributed to 'membrane depolarization' and the decrease in excitability under the cathode is attributed to 'membrane hyperpolarization' (Bindman *et al.* 1964; Purpura & McMurtry, 1965), in fact during DCS there are an equal number of cellular elements that are hyperpolarized or depolarized in any given brain region (Joucla & Yvert, 2009), including directly under the anode and cathode. For example, during DCS of cortical pyramidal neurons, somatic depolarization is associated with concurrent apical dendritic hyperpolarization, and somatic hyperpolarization is associated with apical dendritic depolarization (Chan & Nicholson, 1986; Tranchina & Nicholson, 1986; Chan *et al.* 1988; Andreasen & Nedergaard, 1996; Radman *et al.* 2009). Additionally, afferent axons and their terminals are also polarized during DCS with varied polarity depending on morphology (Ranck, 1975; Tranchina & Nicholson, 1986; Arlotti *et al.* 2012; Kabakov *et al.* 2012; Marquez-Ruiz *et al.* 2012). Finally, membrane compartment-specific polarization affects the capacity of presynaptic input to influence postsynaptic output (synaptic efficacy) in both acute and long-lasting effects of DCS (Bikson *et al.* 2004; Fritsch *et al.* 2010; Kabakov *et al.* 2012; Marquez-Ruiz *et al.* 2012). The diversity of cellular targets of DCS raises a number of mechanistic questions. Which membrane compartments (somas, dendrites or axons/terminals) polarized during DCS contribute to changes in excitability, including synaptic efficacy? Does depolarization/hyperpolarization of the implicated compartments in fact correlate with facilitation/inhibition of synaptic efficacy?

Classical animal research has implicated somatic polarization during transcortical DCS (Terzuolo & Bullock, 1956; Purpura & McMurtry, 1965). Accordingly, local field potentials and intracellular recordings suggest that facilitation/inhibition of spontaneous activity (Frohlich & McCormick, 2010; Reato *et al.* 2010) and synaptic efficacy during DCS may be associated with depolarization/hyperpolarization of the somatic membrane potential (Jefferys, 1981; Bikson *et al.* 2004; Radman *et al.* 2009). However, afferent axons, including corticocortical and thalamocortical connections, which are involved in synaptic processing, might additionally contribute to the effects of DCS (Purpura & McMurtry, 1965; Bikson *et al.* 2004; Kabakov *et al.* 2012; Marquez-Ruiz *et al.* 2012). For example, modulation of presynaptic transmitter release at thalamocortical sensory

afferents has been attributed to the effects of DCS *in vivo* (Marquez-Ruiz *et al.* 2012). Whether hyperpolarization or depolarization of axon terminals enhances efficacy may vary across synaptic pathways. Finally, DCS of the apical dendrites of pyramidal neurons, which polarize opposite to somas, may further influence synaptic processing (Bikson *et al.* 2004). Thus, it remains unclear which compartments influence modulation by DCS (somas, dendrites or axons/terminals), and whether depolarization or hyperpolarization is associated with enhanced synaptic efficacy. Understanding the cellular targets of tDCS is considered pre-requisite to rational electrotherapy design and optimization (Bikson *et al.* 2012*b*).

The well-established approach to characterize the cellular effects of electrical stimulation is to determine the EF produced in the target brain region and then reproduce the EF in animal models or neuron compartment models; for transcranial stimulation, including with DCS, the quasi-uniform assumption is widely applied (Bikson *et al.* 2012*a*). We extended previous magnetic resonance imaging (MRI)-derived models of tDCS-generated brain current flow (Datta *et al.* 2009; Salvador *et al.* 2010) to quantify the directionality of the induced EF in the cortex–specifically the relative radial and tangential components of the cortical EF. In the second part of this study, we aimed to characterize the role of uniform EFs on modulating the excitability of extracellular field potentials using brain slices, which facilitate control of EF direction (radial and tangential to the somatodendritic axis) and isolated activation of pathway-specific synaptic activity. Finally, compartment models of morphologically reconstructed cortical pyramidal neurons were used to predict which neuronal elements are polarized by uniform DC fields.

We report that during tDCS both radial and tangential (relative to the cortical surface) direction currents are induced; however, tangential currents are prevalent across the cortex. Fields radial to the cortical surface modulated synaptic efficacy independent of the synaptic pathway and consistent with somatic polarization, with depolarization/hyperpolarization facilitating/inhibiting synaptic efficacy, while tangential fields modulated synaptic efficacy in a pathway-specific manner, such that axon terminal hyperpolarization/depolarization was associated with facilitation/inhibition of synaptic efficacy. The acute effects of DCS on synaptic efficacy may be reconciled through (concurrent) contributions from these two cellular targets.

Methods

MRI-derived EF models

Complete methods for MRI-derived head models of EF distributions are detailed elsewhere (Datta *et al.* 2009). Briefly, EF distributions in the brain were computed using individualized head models created from the T1-weighted MRI scans of a healthy individual. The head was segmented into compartments representing grey matter, white matter, cerebrospinal fluid, skull, scalp, eye region, muscle, air and blood vessels using a combination of tools from the FSL and Simpleware (Exeter, UK). The finite element (FE) mesh generated from the segmentation masks was exported to COMSOL Multiphysics 4.2 (Burlington, MA, USA) for computation of EFs.

EF magnitudes were calculated for the conventional tDCS montage over M1-SO (one anode over the primary motor cortex and one cathode over the supraorbital region, 5 × 5 cm sponge electrodes; Figs 1*Aa* and 2*A*)and the high-definition tDCS (HD-tDCS) montage (centre anode over the primary motor cortex and four surround cathode electrodes, 1 cm electrode diameter with 6 cm separation between the centre and surround electrodes; Datta *et al.* 2009). The relative magnitudes of the two components of the EF (E_x = radial and E_y = tangential) are considered and quantified on multiple scales (Fig. 2), including global field distributions in the brain, regionally under/between electrodes, and in subregions on gyral crowns/walls. We use the ratio of tangential to radial (E_y/E_x) field magnitudes to describe the relative magnitudes in each region, such that E_y/E_x 1 corresponds to greater tangential fields on average and $E_y/E_x < 1$ corresponds to greater radial fields on average (Fig. 1*Ab* and *Ac*). The E_y/E_x metric is represented in Fig. 1*Aa* with a schematic representation of the voltage distribution overlaid on each region of interest along a cortical gyrus.

Ethical approval

All animal experiments were carried out in accordance with guidelines and protocols approved by the Institutional Animal Care and Use Committee (IACUC) at The City College of New York, CUNY (Protocol No: 846.3).

Electrophysiology

Brain slices including a part of the motor cortex were prepared from male young adult Wistar rats aged 3–6 weeks old, which were deeply anaesthetized with ketamine (7.4 mg kg^{-1}) and xylazine (0.7 mg kg^{-1}) applied I.P., and killed by cervical dislocation. The brain was removed and immersed in chilled (2–6°C) artificial cerebrospinal fluid (ACSF) containing (in mM): NaCl, 126; KCl, 3; NaH_2PO_4, 1.25; $MgSO_4$, 2; CaCl, 2; $NaHCO_3$, 24; D-glucose, 10; bubbled with a mixture of 95% O_2–5% CO_2). Parasagittal slices (450 μm thick) were cut at a distance of 2.0–3.0 mm from the brain midline using a vibrating microtome and transferred to a holding chamber for at least 1 h at ambient temperature. Slices were then transferred to a fluid–gas interface chamber perfused with warmed

ACSF ($30.0 \pm 0.5^{\circ}$C) at 1.9 ml min^{-1}. The humidified atmosphere over the slices was saturated with a mixture of 95% O_2–5% CO_2. Recordings started 2–3 h after dissection.

To investigate the role of distinct cortical pathways on modulation of synaptic efficacy, the recording electrode (a glass micropipette filled with 0.25 M NaCl, resistance 1–8 MΩ) was placed in either layer II/III or layer V

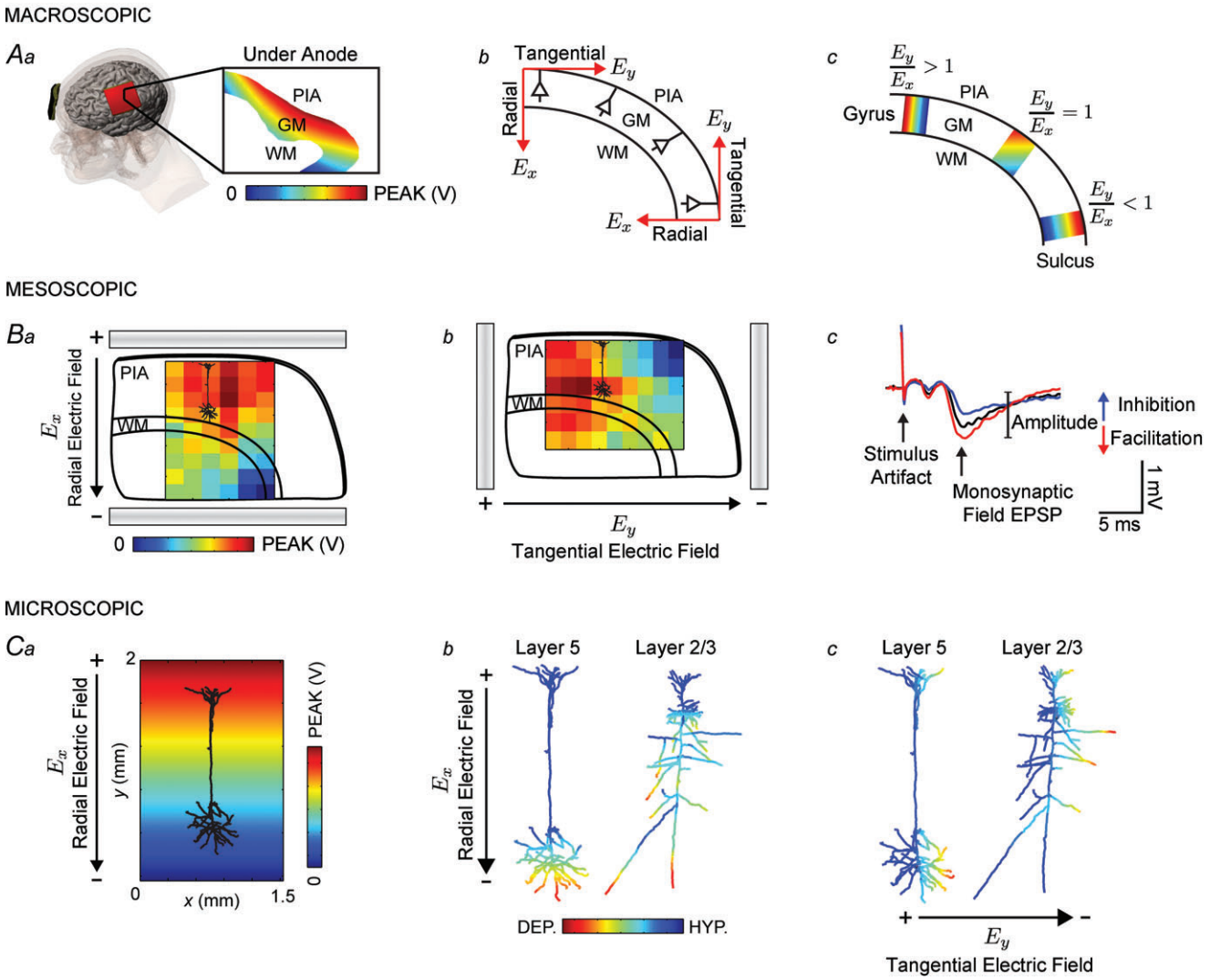

Figure 1. Multi-scale methods and outcome measures of uniform EF directionality and effects
Aa, gyri-precise FEMs of current flow during tDCS indicate a uniform voltage gradient in cortical grey matter (GM) directly under the anode. *Ab*, the induced EF in the cortex can be decomposed into a radial component (E_x) that is parallel to the somatodendritic axis, and a tangential component (E_y) that is orthogonal to the somatodendritic axis. *Ac*, we quantified the relative occurrence of radial and tangential fields in cortical GM expressed as the ratio of the average of the field magnitude in the tangential direction to the average of the field magnitude in the radial direction (E_y/E_x). *Ba* and *b*, the brain slice preparation was used to study the change in synaptic efficacy during a uniform radial or tangential field by recording evoked field potentials. The voltage gradient between parallel Ag–AgCl wires is superimposed on a schematic of a sagittal slice of the rat primary motor cortex. From the macroscopic to the mesoscopic scale we can approximate a uniform EF along the length of a neuron (compare voltage gradients in *Aa* and *Ba*). *Bc*, the field (f)EPSP provides a measure of synaptic efficacy through facilitation or inhibition of the response amplitude. *Ca*, compartment model simulations of morphologically reconstructed neocortical pyramidal neurons were used to provide a description of axon terminal polarization in a uniform EF. *Cb*, the polarization profile of a layer V pyramidal neuron in a radially directed uniform EF indicating soma depolarization (red) corresponds to apical dendrite hyperpolarization (blue). Layer II/III neurons have a more complex polarization profile with long processes reaching maximal depolarization independent of the neuronal body. *Cc*, neurons in a uniform EF directed tangential to the somatodendritic axis preferentially affect processes that are oriented along the tangential field. WM, white matter.

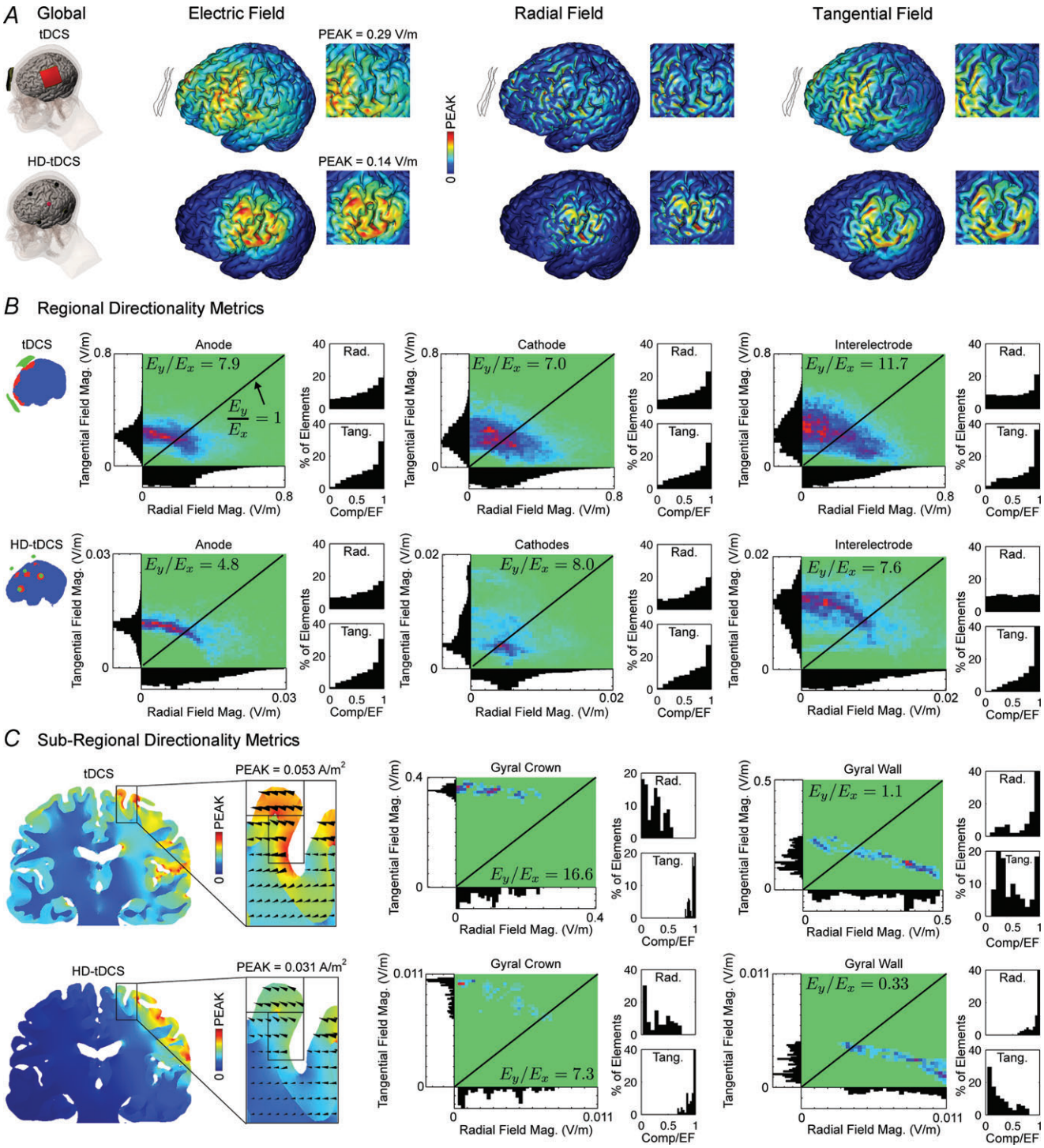

Figure 2. Forward model of transcranial direct current stimulation (tDCS) and high-definition (HD)-tDCS quantifying electric field (EF) direction metrics

During tDCS, current may be dominantly tangential (along the cortical surface) rather than radial, even in brain regions directly under the electrodes. *A*, MRI-derived FEMs of current distribution in a gyri-precise head model are used to quantify the relative occurrence of radial (normal to the cortical surface) and tangential (along the cortical surface) components of the EF. Both conventional (top) and HD (bottom) tDCS montages produce radial (E_x, normal to the cortical surface) and tangential current (E_y, along the cortical surface) indicated by the global EF distribution (V m^{-1}) across the head. In the HD-tDCS montage, current is focalized within the ring configuration (inset) with radial currents under the centre electrode and tangential currents between the surround electrodes. Qualitative comparison of the EF components indicates greater radial field magnitudes in the gyral wall and greater tangential field magnitudes in the gyral crown (compare insets). *B*, regionally, the distribution of field component

of the rat primary motor cortex (Fig. 3*A*). Neocortical horizontal pathways (within a cortical layer) and vertical pathways (across lamina) represent functionally distinct connections that are well characterized in the rat neocortex (Aroniadou & Keller, 1993; Keller, 1993). For instance, horizontal connections integrate information across sensory maps in the motor cortex by connecting related functional columns; however, extrinsic connections from distant cortical and subcortical regions have dominantly vertical projections (Hess & Donoghue, 1994). The synaptic circuits representing intrinsic connections between populations of neurons within the motor cortex were previously identified in the literature using current source density distributions, morphological analysis and through studies of functional connectivity, including long-term potentiation and depression experiments (Aroniadou & Keller, 1993, 1995; Keller, 1993; Castro-Alamancos *et al.* 1995; Hess *et al.* 1996; Rioult-Pedotti *et al.* 1998). Figure 3*B* summarizes the identified pathways relevant for this study. In addition to probing the pathway-specific effects of EFs on cortical field potentials, we use the synaptic organization of the cortex to test the effectiveness of radial and tangential fields in modulating synaptic efficacy in horizontal and vertical pathways.

Orthodromic stimulation targeting four distinct synaptic pathways previously identified in the rat primary motor cortex was applied with a bipolar platinum/stainless steel stimulating electrode placed either 400–800 μm (stimulating electrodes S1 and S2) or 1100–1300 μm (stimulating electrodes S3 and S4) below the pial surface to activate fibres running within layer II/III or layer V, respectively (Fig. 3*A*). The stimulating electrodes were placed either laterally anterior or posterior to the recording electrode targeting horizontal afferent synaptic connections in either of the superficial (S1 and S2) or deep layers (S3; Fig. 3*A*). Vertical connections were stimulated with a bipolar electrode (S4) in deep layer V and a recording electrode in layer II/III. Field EPSPs (fEPSPs), which provide a measure of localized extracellular currents generated from a population of pyramidal neurons in response to synaptic or antidromic activation, were evoked with constant-current pulses (0.2 ms) delivered once per minute. The test stimulus intensity (30–200 μA) was adjusted to evoke half-maximal responses based on input–output curves (Fig. 4*A*); no consistent relationship was found between fEPSP delay and stimulation amplitude or fEPSP peak. This relatively weak stimulation did not evoke population spikes, and usually elicited a fEPSP having a single peak in 84 of 92 slices tested. Responses were amplified, low-pass filtered (1000 Hz cutoff; Warner Instruments, CT, USA), acquired at a 10 kHz sampling rate (1401 interface, CED, UK), and analysed on- and offline (Signal 3 software, CED, UK).

The stimulation protocol was designed to measure the acute (during field) changes in fEPSPs evoked during an applied EF. fEPSP amplitudes were used as a measure of the change in synaptic efficacy during the field, such that an increase in the amplitude indicates facilitation and a decrease indicates inhibition. Uniform fields ($\pm$8 V m^{-1}) were generated by passing current (D/A driven analog current follower; A-M Systems, WA, USA) between two large parallel Ag–AgCl wires positioned in the bath across the slice for 1 s starting 0.5 s before bipolar stimulation. The field intensity was chosen based on pilot experiments to produce approximately a 5% change in fEPSP amplitude such that a statistically significant change could be observed within slices with a practical sample size (Fig. 4*B*).

The quasi-uniform EF assumption (Bikson *et al.* 2012*a*), which considers the applied EF amplitude may be uniform on the scale of the membrane length constant, allowed us to evaluate synaptic efficacy in a population of neurons in a uniform EF *in vitro* as well as in single neuron models (compare Fig. 1*Aa*, *Ba* and *Ca*). Specifically, tDCS produces approximate uniform fields across select regions of grey matter (Fig. 1*A*, linear voltage gradients) that can be reproduced *in vitro* (Fig. 1*B*) and simulated *in silico* (Fig. 1*C*). Consideration of uniform EFs allows analysis in this study across the macroscopic (brain current flow using the FE model (M)), mesoscopic (synaptic efficacy in brain slice) and microscopic scales (neuron compartment polarization). Indeed, representation of EFs is ubiquitous in FEM computational studies (Miranda *et al.* 2006; Datta *et al.* 2009, 2011; Salvador *et al.* 2010), and uniform EFs are used in mechanistic studies of tDCS (Radman *et al.*

magnitudes indicates prevailing tangential currents under the anode, cathode and between electrodes as described by the ratio of tangential to radial field magnitude (E_y/E_x ratio, see Methods). However, most elements have both radial and tangential components, and the isolated highest EFs are radial. The tangential and radial component for individual elements is shown for each subregion in false colour density plots, which show relative occurrence (relative density from absent (green) to maximal (red)). Axis histograms show the relative distribution of elements with a given tangential or radial component EF. Inset histograms describe the distribution of the percentage of elements in a region as a function of the normalized component magnitude (such that 1 indicates elements with dominant radial or tangential component). *C*, cortical folding further influences the distribution of the EF, therefore, subregional field component distributions are indicated for a gyral crown and wall. Tangential fields are dominant in magnitude in the gyral crown but are weaker in the walls where radial magnitudes are stronger, as observed in *A*.

2009; Anastassiou *et al.* 2010; Fritsch *et al.* 2010; Arlotti *et al.* 2012; Kabakov *et al.* 2012; Ranieri *et al.* 2012). To our knowledge this is the first study to integrate analysis across these three scales.

All the statistical data are expressed as mean ± SD, unless stated otherwise. The statistical difference between groups (critical value = 0.05) was estimated using the Student's *t* test considering normally distributed fEPSP amplitudes (Lilliefors test for normality).

Compartment model simulation

Numerical and analytical solutions of 3D reconstructed neurons and simplified cable models, respectively, were used to infer a general rule of steady-state axon terminal polarization under a uniform EF based on axonal morphology. With thousands of axonal afferents, with diverse morphologies for any given cortical neuron, a range of axon terminal polarization values is expected, but our goal was to approximate the *maximum* polarization expected in the most sensitive axon terminals. Specifically, we aimed to characterize the sensitivity of axon terminals by their coupling constant (which linearly relates steady-state membrane polarization to EF), this then allows comparison of maximal axon terminal sensitivity with previously characterized coupling constants for neuron somas (Radman *et al.* 2009).

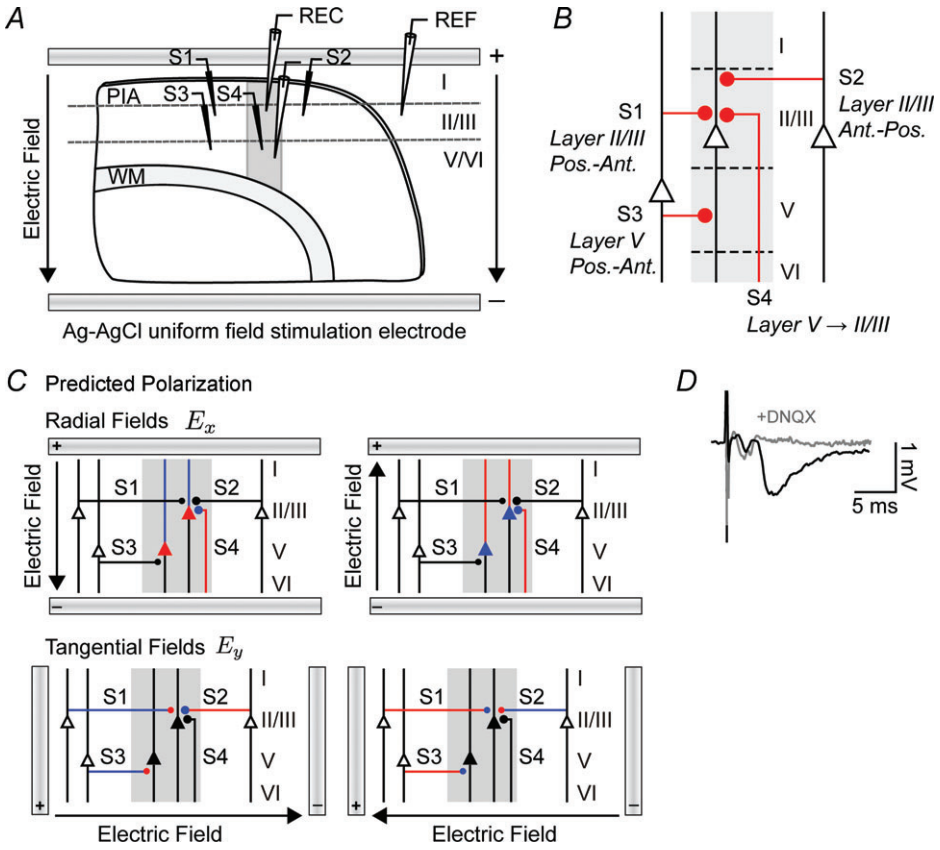

Figure 3. Electrophysiology of direction-specific uniform DC EFs in synaptic pathways of the rat motor cortex

A, schematic of electrophysiology setup where uniform extracellular EFs were generated in all experiments by passing constant current across parallel Ag–AgCl wires positioned in the bath across the slice. Activity was monitored in layer II/III or layer V with a glass microelectrode. An additional field electrode (REF) was positioned in an iso-potential to remove the uniform field artifact. Activity was evoked with a bipolar stimulating electrode (S1–S4) positioned 500 μm from the recording electrode in either layer II/III or layer V targeting one of four distinct synaptic pathways corresponding to different orientations of afferent axons: posterior horizontal layer II/III (S1); anterior horizontal layer II/III (S2); posterior horizontal layer V (S3); and vertical layer V to II/III (S4). *B*, diagram summarizing the primary synaptic circuits in this study. Line thicknesses and diameters of the filled circles, which represent synapses, are correlated with the strength of the synaptic input. *C*, schematic of the expected polarization in distinct synaptic pathways exposed to radial and tangential fields. Somas, dendrites, axons and axon terminals are depolarized (red), hyperpolarized (blue) or not affected (black) by DC fields. *D*, characteristic fEPSP and field spike waveforms from the layer V pathway. The fEPSPs, but not earlier field spike, were suppressed by the non-NMDA receptor antagonist 6,7-dinitroquinoxaline-2,3-dione (DNQX). WM, white matter.

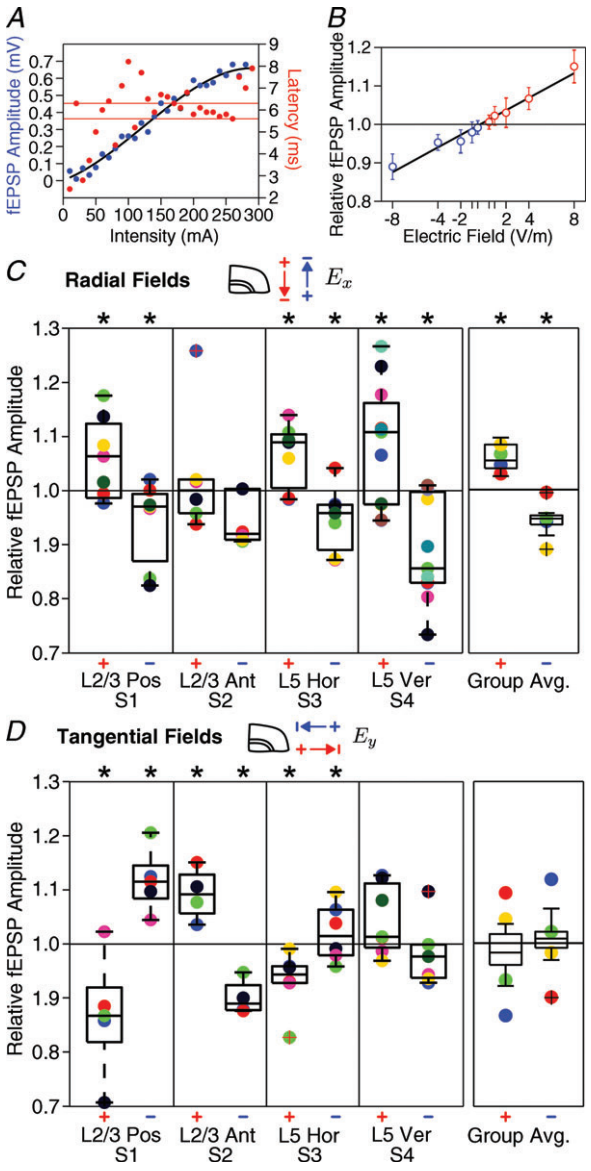

Figure 4. Modulation of pathway-specific synaptic efficacy by radial and tangential DC fields
Application of DC currents in cortical slice demonstrates that tangential currents are as effective in modulating pathway-specific synaptic efficacy as radial currents, though pathway-average effects result only for radial EFs. *A*, input–output curve of field (f)EPSP response amplitude and peak latency in the horizontal layer V pathway. Horizontal grey bars indicate the 25th and 75th percentiles of fEPSP peak latency. *B*, relative fEPSP amplitude in the vertical layer V to II/III pathway at different radially oriented EF intensities (correlation coefficient R^2 of linear fit = 0.96). The fEPSP waveform inset shows a characteristic change in fEPSP amplitude with positive (+8 V m^{-1}, red) and negative radial fields (−8 V m^{-1}, blue) from control (no field, black). *C*, fEPSP responses are significantly (*$P < 0.05$) facilitated with +8 V m^{-1} fields (left) and reduced with −8 V m^{-1} (right) in three pathways. In each pathway, individual slice averages are indicated with coloured circles. Grouped average fEPSP amplitudes across all synaptic pathways indicate a 7% polarity-specific modulation of synaptic efficacy with 8 V m^{-1} radial fields. Circles in the grouped average represent the across slice means of distinct pathways (blue, red, green and yellow are S1, S2, S3 and S4 pathways, respectively). *D*, fEPSP amplitude was significantly modulated by tangential EFs in all three horizontal pathways but with direction sensitivity and not in the vertical pathway, all consistent with terminal polarization. Although tangential fields affected individual pathways, the grouped average of fEPSP amplitudes across all pathways was not significant.

Numerical solutions for realistic neurons. Complex neuronal geometries require numerically solving the cable equation (Basser & Roth, 2000). Eight morphologically reconstructed layer II/III and layer V rat somatosensory pyramidal neurons from the NeuroMorpho.org database (ID: NMO_0116, NMO_00348, NMO_00410, NMO_00417, NMO_01134, NMO_01132, NMO_01135, NMO_01112) were used to approximate membrane polarization in a uniform EF using Neuron (version 7.2; Wang *et al.* 2002; Ascoli, 2006). The built-in function extracellular(x) was used to apply 1 V m^{-1} uniform EFs in the radial direction (parallel to the somatodendritic axis; Fig. 1*Ca* and *Cb*), tangential direction (perpendicular to the somatodendritic axis; Fig. 1*Cc*) and at optimal polarization angles along individual axons to produce the maximum terminal polarization in that axon. The membrane resistance R_m was 70 kΩ cm^{-2} and the intracellular axial resistance R_i was 155 Ω cm^{-1} (Markram *et al.* 1998). The median axonal length constant ($\lambda = \sqrt{\frac{r \times \rho_m}{2 \times \rho_i}}$, where r is the radius, ρ_m is the membrane resistivity and ρ_i is the intracellular resistivity) was 0.56 mm (0.05 mm interquartile range). In all compartment neuron models, passive resistive parameters were used to approximate steady-state membrane polarization.

Branched semi-infinite axon. Next, we considered a bent semi-infinite axon in a uniform EF to establish a relationship between terminal polarization and fibre morphology, extending previous derivations (Tranchina & Nicholson, 1986; Basser & Roth, 2000; Miranda *et al.* 2007). We previously derived the analytical steady-state solution to the classic cable equation for a passive terminating straight branch of an axon (eqn (1); for a complete derivation, see Arlotti *et al.* 2012).

$$V_t = E\lambda\cos(\theta)\tanh(\ell/\lambda) + V_0\frac{1}{\cosh(\ell/\lambda)} \qquad (1)$$

The terminal polarization varies with the physical length ℓ of the final segment and depends on the angle θ of the EF, E, relative to the final branch and the membrane polarization at the bend V_0. The relative contribution of $E\lambda$ *vs.* V_0 depends on the electrotonic (dimensionless) length ℓ/λ.

Straight semi-infinite axon. A simple analytical solution of polarization of a straight semi-infinite axon in a uniform EF is well known (and is in fact a special case of the axon branch with infinite length); eqn (2) relates polarization at the fibre terminal with the membrane space constant λ (Hause, 1975). The terminal membrane polarization is a function of the uniform extracellular EF relative to the axon, such that $\theta = 0$ corresponds to an EF along the longitudinal axis of the fibre. Interestingly, in this formulation λ is analogous to the coupling constant, and we intend to establish if and when this approximation is valid for realistic axon morphologies.

$$\ell \gg \lambda \Rightarrow V_t = E\lambda\cos\theta \quad (2)$$

Results

The overall goal of this study was to systematically characterize the cellular target of action for DCS. Our approach was to first determine the prevalence of radial and tangential EFs in the cortex using MRI-derived computational models. Secondly, the effects of radial and tangential DC fields on synaptic efficacy were characterized in cortical brain slices in four distinct synaptic pathways corresponding to different orientations of afferent axons. Synaptic efficacy was shown to be pathway specific, and synaptic terminal polarization by tangential fields can lead to facilitation/inhibition independent of somatic polarization. These findings motivated us to determine a general rule to describe sensitivity of axon terminals to polarization in the form of a coupling constant.

Quantitative analysis of EF directionality in FEMs of tDCS and HD-tDCS

Consistent with previous computational studies, tDCS and HD-tDCS are predicted to generate weak EFs ($<1\ \mathrm{V\,m^{-1}}$ per mA applied current) in the cortex, with a complex spatial pattern determined by the electrode montage and the details of brain anatomy, notably cortical surface idiosyncrasies (Datta *et al.* 2009). Under the assumption that the voltage gradient in each region of the grey matter was locally linear, we summarized the (uniform) EF in each region (Figs 1*A* and 2). Cortical EFs generated during stimulation have components both radial (E_x, normal) and tangential (E_y, parallel) to the cortical surface (Fig. 1*B*). Radial fields that are oriented along the somatodendritic axis of cortical pyramidal neurons produce somatic polarization. Tangential fields are transverse to the somatodendritic axis of cortical pyramids, and will polarize horizontally directed cortico-cortical axons. High-resolution modelling shows that current flowing across the grey matter will have both radial and tangential components in conventional (Fig. 2*A*, top) and HD- (Fig. 2*A*, bottom) tDCS. We previously reported interindividual variations of peak cortical EF of ∼twofold across anatomically normal adult heads (Datta *et al.* 2012), but focus here on relative directional distribution. The global prevalence of tangential fields motivated further analysis of field directionality on additional levels, including regions under/between electrodes and sub-regions of gyral crown/walls.

The distribution of radial and tangential components (Fig. 2*B*; density plots show relative occurrence) under the anode (E_y/E_x tDCS: 7.9; HD-tDCS: 4.8), cathode (E_y/E_x tDCS: 7.0; HD-tDCS: 8.0) and between electrodes (E_y/E_x tDCS: 11.7; HD-tDCS: 7.6) indicates most elements have both field components, but with (significantly) stronger tangential than radial field (Fig. 2*B*, inset histograms). Interestingly, the few isolated highest EFs are radial (Fig. 2*B*, axis histograms).

Cortical folding greatly influenced the EF distribution under the electrodes (Fig. 2*C*). For example, on the scale of a single gyrus in the primary motor strip, the gyral crown has a dominantly tangential component (E_y/E_x tDCS: 16.6; HD-tDCS: 7.3) and the strongest fields are tangentially oriented. In contrast, motor strip gyral walls have a relatively equal distribution of field components using the conventional tDCS electrode montage and slightly stronger radial components in HD-tDCS (E_y/E_x tDCS: 1.1; HD-tDCS: 0.33). The maximal EF in gyral walls is typically radial to the cortical surface, but a few elements have negligible tangential components as well.

In all regions, under and between electrodes, there is a higher density of elements with stronger tangential than radial fields, and few elements had purely radially oriented fields. Given the prevalence of tangential EFs, we next considered field direction-sensitive changes in synaptic efficacy in cortical pathways of the rat primary motor cortex.

Effects of EFs applied parallel and perpendicular to the somatodendritic axis on cortical field potentials

The primary motor cortex is characterized by functionally distinct afferent synaptic pathways with specific axonal morphologies and orientations (Aroniadou & Keller, 1993; Keller, 1993). Using the rat primary motor cortex slice preparation we tested the acute effects of uniform EFs on synaptic efficacy in four distinct cortical pathways for EFs applied parallel to the somatodendritic axis (radial fields) and perpendicular to the somatodendritic axis (tangential fields). fEPSPs were monitored in layer II/III or layer V in response to activity evoked by stimulation of posterior or anterior afferent synaptic pathways in layer II/III (stimulating electrodes S1 and

S2, respectively) and horizontal or vertical afferents in layer V (stimulating electrodes S3 and S4, respectively; Fig. 3*A* and *B*). In addition to monosynaptic fEPSPs (4–7 ms peak), a fibre volley was observed in some slices that was non-synaptically mediated, as indicated by the time course (<2 ms peak) and insensitivity to bath application of the non-NMDA receptor antagonist 6,7-dinitroquinoxaline-2,3-dione (DNQX; 20 μM; Fig. 3*D*). We tested the hypothesis that synaptic efficacy increases with somatic depolarization and/or axon terminal hyperpolarization, thus in a defined polarity, field direction and pathway-specific manner (Fig. 3*C*).

Radial EFs (parallel to the somatodendritic axis of cortical pyramidal neurons) typically lead to 'excitation' for positive fields (anode proximal to pia) and 'inhibition' for negative fields (cathode proximal to pia; Fig. 1*B3*). In three of the afferent pathways tested, fEPSP amplitudes were significantly facilitated (Fig. 4*C*; S1: posterior horizontal layer II/III, $5.2 \pm 3\%$, $P = 0.031$, $n = 7$; S3: horizontal layer V, $7.3 \pm 8\%$, $P = 0.02$, $n = 7$; S4: vertical layer II/III, $9.4 \pm 4\%$, $P = 0.023$, $n = 11$) by radial positive EFs ($+8$ V m^{-1}), with no significant effect in one pathway (S2: anterior horizontal layer II/III, $P = 0.251$, $n = 6$). Radial negative fields (-8 V m^{-1}) reduced responses in the same three pathways (S1: $-8 \pm 1\%$, $P = 0.022$, $n = 7$; S3: $-6.4 \pm 6.9\%$, $P = 0.024$, $n = 7$; S4: $-10.2 \pm 1.5\%$, $P = 0.01$, $n = 11$), with no significant effect in the anterior horizontal layer II/III pathway (S2: $P = 0.98$, $n = 6$). A change in fEPSP timing was not resolved. Importantly, grouping across all pathways (e.g. not controlling pathway selectivity), 8 V m^{-1} radial positive fields significantly facilitated ($7 \pm 1\%$, $P = 0.004$) and radial negative fields inhibited ($-6.1 \pm 4\%$, $P = 0.04$) fEPSP amplitudes (Fig. 4*C*).

tDCS also induces tangential fields that are not expected to polarize neurons with a somatodendritic axis radial to the cortical surface (Fig. 3*C*; Bikson *et al.* 2006). Yet, we found tangential positive fields significantly modulated three out of four pathways tested; moreover, the direction of change in excitability was pathway specific. Tangential positive fields ($+8$ V m^{-1}, oriented posterior to anterior) reduced fEPSP responses in two pathways (Fig. 4*D*; S1: posterior horizontal layer II/III, $-10 \pm 3.7\%$, $P = 0.024$, $n = 5$; S3: posterior horizontal layer V, $-5.6 \pm 4\%$, $P = 0.01$, $n = 6$), facilitated in one pathway (S2: anterior horizontal layer II/III, $9.7 \pm 2\%$, $P = 0.02$, $n = 4$), and had no significant effect on the fourth pathway (S4: vertical layer II/III, $P = 0.14$, $n = 7$). Tangential negative fields (-8 V m^{-1}, oriented anterior to posterior) facilitated responses in all horizontal pathways (S1: posterior horizontal layer II/III, $11.4 \pm 2.5\%$, $P = 0.007$, $n = 5$; S2: anterior layer II/III, $-10.3 \pm 3\%$, $P = 0.009$, $n = 4$; S3: posterior horizontal layer V, $4.3 \pm 6.9\%$, $P = 0.024$, $n = 6$), with no significant modulation of synaptic efficacy in the vertical pathway (S4: vertical layer II/III, $P = 0.13$, $n = 7$). Across modulated afferent pathways, our results are consistent with tangential EFs that produce synaptic terminal hyperpolarization/depolarization leading to facilitation/inhibition of synaptic efficacy (compare Figs 3*C* and 4*D*). Though individual pathways were generally as sensitive to tangential fields as radial fields, tangential EFs had no *average* effect on synaptic efficacy averaging across pathways by virtue of anterior- and posterior-directed afferents (Fig. 4*D*). Afferent axon terminal polarization by subthreshold DC fields was next explored using compartment models to understand morphological factors influencing terminal polarization.

Polarization of axon terminals in compartment neuron models

Synaptic terminal polarization by a uniform extracellular EF leads to changes in synaptic efficacy, consistent with observations in cortical brain slices. Therefore, we estimated the polarization of axonal terminals to weak DCS using compartment and analytical models. The sensitivity of a given compartment to a subthreshold field can be expressed as the coupling constant (or polarization length) in terms of membrane polarization per unit EF (mV per V m^{-1}; Bikson *et al.* 2004; Radman *et al.* 2009).

The relative terminal polarization was calculated numerically for fields oriented parallel (radial component of EF; Fig. 1*Cb*) or perpendicular (tangential component of EF; Fig. 1*Cc*) to the somatodendritic axis, as well as for fields oriented in the optimal angle that leads to maximal polarization at each terminal (Fig. 5*A* and *B*). Layer V neurons with passive properties exposed to a strong uniform EF produce a bimodal polarization profile (Fig. 1*Cb*; false colour indicates relative depolarization (red) and hyperpolarization (blue)). However, layer II/III neurons demonstrate a complex polarization profile with distal axonal branches approaching maximal polarization at the terminals independently of the polarization along the neuronal axis (Figs 1*Cb*–c). Cortical axons are not straight even over microscopic scales, but we considered the length of each terminating branch as the distance from the terminal to the bend (Fig. 5*A*). The final branch space constant varied with fibre radius. We considered relative terminal polarization (V_t normalized by the axonal length constant and by EF) to indicate sensitivity compared with the semi-infinite axon case (maximal polarization = $E\lambda$). For radial and tangential EFs, numerical simulations of cortical neuron polarization indicated that terminal polarization was a complex function of neuronal morphology and angle relative to the EF. Though varying within ± 1 (i.e. $\pm E\lambda$), there was no apparent monotonic relationship between the terminal coupling constant and branch length (Fig. 5*A*, *Ba* and *Bb*). However, further consideration of branch angle

reveals that, specifically for long branches, relative terminal polarization approaches ± 1 for branches oriented parallel to the EF and ∼0 for branches perpendicular to the EF:

$$V_t(\theta, \ell \gg \lambda) = \begin{cases} E\lambda & \text{if } \theta = 0^\circ \\ 0 & \text{if } \theta = 90^\circ \\ -E\lambda & \text{if } \theta = 180^\circ \end{cases} \quad (3)$$

Moreover, when considering the optimal polarization angle, the relative axon terminal polarization asymptotically approaches a magnitude of 1 with increasing branch length (Fig. 5*Bc*).

The analytical solution for a bent axon (eqn (1)) was derived from the cable equation to describe the relationship between axon morphology and terminal coupling constant. For branched axons (Fig. 5*Ca*), the terminal polarization is the sum of: (1) the polarization at the branch point (V_0) weighted by the inverse of the final segment's electrotonic length; and (2) $E\lambda$, considering the component of EF along the final segment, weighted by the final segment's electronic length. For short branches the terminal membrane potential is coupled with the membrane potential at the bend (V_0) and therefore depends on overall neuronal morphology and where the segment connects to the overall structure (Fig. 5*Ba* and *Bb*, note the variability for short branch lengths). For long branches, where $\ell \gg \lambda$, the terminal membrane potential becomes independent of the branch point and approaches $E\lambda\cos\theta$. Eqn (1) (using numerically determined branch point voltage) was verified for numerically calculated

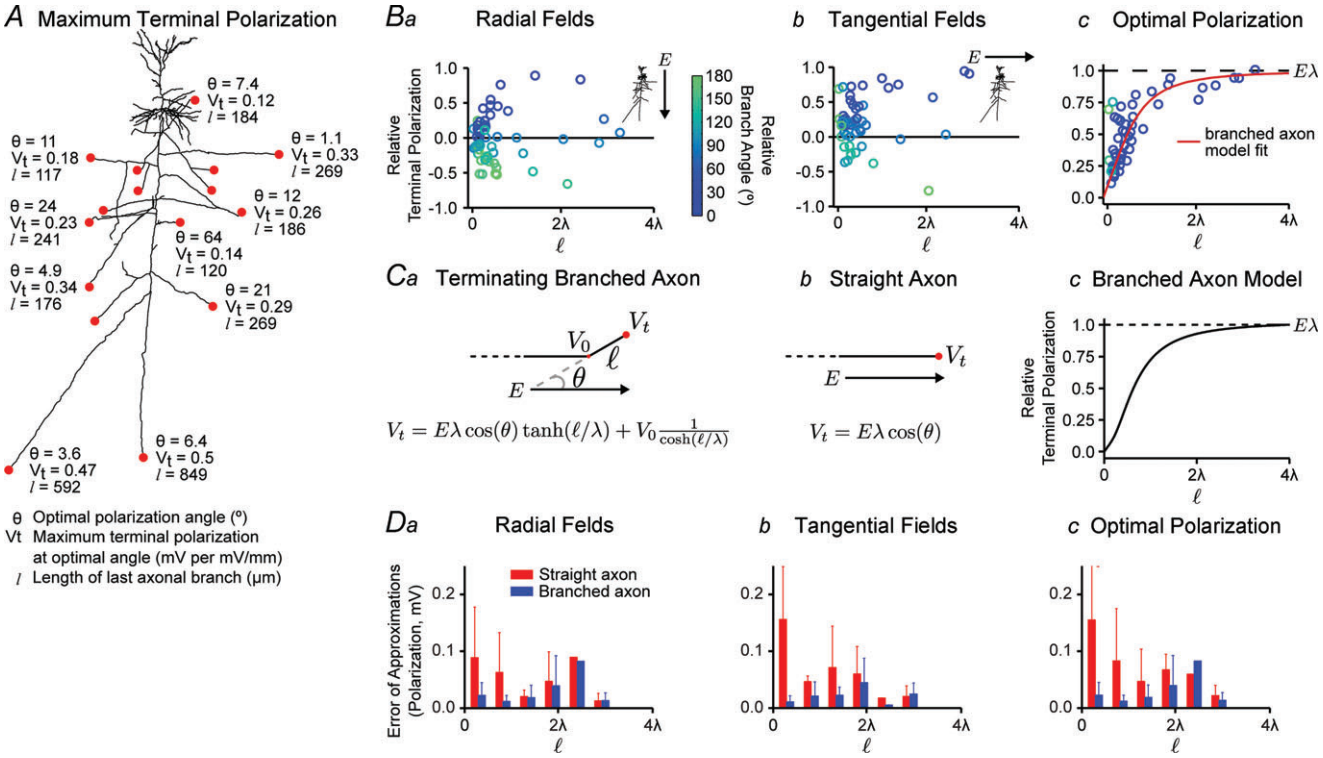

Figure 5. Terminal polarization by uniform DC EFs using neuron compartment model and analytical/hybrid approximations
The maximum terminal polarization (V_t) depends on the length (ℓ) of the last axonal branch and becomes uncoupled from the bend point at distant terminals ($\ell > 3\lambda$); however, for short branches the terminal membrane potential is coupled with the membrane potential at the bend (V_0). In all cases, numerical simulations applied 1 V m^{-1} EFs. *A*, for a typical cortical pyramidal neuron, the maximum terminal polarization (V_t) is plotted with the corresponding optimal polarization angle (θ) of the branch relative to the EF and the length (ℓ) of the terminating axon branch. *Ba* and *b*, relative terminal polarization (V_t normalized by the axonal length constant and by the EF) as a function of branch electrotonic length and angle (circle colour). *Bc*, considering the optimal polarization angle, the relative polarization asymptotically approaches magnitude 1 with branch length (equivalently, terminal polarization reaches the maximal polarization $E\lambda$ for increasing lengths). *Ca* and *b*, schematic of a branched and straight axon in a uniform EF with analytical solutions (see Methods). The straight axon is a special case of the branched axon with infinite final branch length. For long branches, where $\ell \gg \lambda$, the terminal membrane potential becomes independent of the branch point and approaches $E\lambda\cos\theta$. *Cc*, the branched axon model approaches maximal terminal polarization $E\lambda$ for $\ell > 3\lambda$. *D*, error of approximations (analytical *versus* numerical estimates) for branched (blue) and straight (red) axons.

terminal polarization (Fig. 5*D*). For the case of final segments oriented parallel to the EF, eqn (2) predicts an asymptotic approach to $E\lambda$ for final branch lengths $>3\lambda$, consistent with numerical simulations (Fig. 5*Bc*). Eqn (2) thus explains how overall neuron geometry *versus* axon terminal morphology affects resulting terminal polarization, and how maximum expected polarization at a terminal would be $E\lambda$ for a sufficiently long final branch oriented along the field (Fig. 5*Bc* and *Cc*). Importantly, given the density and diversity of afferent axons in the cortex (some with long optimally oriented final branches), it is reasonable to predict some axon terminals reach the maximal polarization $E\lambda$ for *any* given EF orientation.

The relevance of the idealized straight semi-infinite axon (Fig. 5*C*), which can be described by a simple analytical solution ($V_t = E\lambda\cos\theta$ or $E\lambda$ for fields oriented along the branch), to realistic tortuous cortical axon morphologies can now be explained with the relationship we have derived (see above). This approximation is relevant for the cases of the branched axon where the final semi-straight segments' electrotonic length is sufficiently long ($>3\lambda$); these are also the most sensitive terminals to polarization by EFs. Thus, the membrane length constant λ reflects the maximal coupling constant of afferent axonal terminals.

Discussion

The application of tDCS in both clinical and cognitive-neuroscience research has been encouraged by the simplicity of the technique (two electrodes and a battery-powered stimulator) and the perception that tDCS protocols can be designed by placing the anode/cathode over the cortex to 'excite/inhibit'. The mechanistic question of how acute DCS modulates excitability and ongoing neuronal activity depends on the affected cellular targets.

We characterized DCS-generated EFs, how they polarize cellular compartments, and in turn modulate synaptic efficacy; our approach applied the quasi-uniform assumption (Bikson *et al.* 2012*a*) to link FEMs of cortical current flow, brain slices and neuron compartment models (Fig. 1). On the basis of our findings, the overarching framework we propose is: during tDCS current crosses the cortex with an EF vector containing dominantly tangential but also radial components (relative to the cortical surface), whereas the radial component will facilitate/inhibit synaptic efficacy through somatic depolarization/hyperpolarization, the tangential component will concurrently facilitate/inhibit synaptic efficacy, in a pathway-specific manner, through terminal hyperpolarization/depolarization. The rationale for this framework in the context of prior mechanistic studies is considered.

Somatic polarization mediates modulation of synaptic efficacy by radial cortical current flow

Animal studies of DCS on spontaneous and evoked cortical activity (Creutzfeldt *et al.* 1962; Purpura & McMurtry, 1965; Jefferys, 1981; Chan & Nicholson, 1986; Chan *et al.* 1988; Gluckman *et al.* 1996; Fritsch *et al.* 2010; Reato *et al.* 2010) demonstrate that typically surface-anode stimulation increases activity while surface-cathode decreases activity, consistent with somatic membrane polarization (Radman *et al.* 2009). Similar principles apply in the hippocampus after considering the inverted pyramidal neuron morphology (Gluckman *et al.* 1996; Bikson *et al.* 2004; Kabakov *et al.* 2012). In classical animal studies, by virtue of the stimulation technique (e.g. invasive electrode) and/or cortical anatomy (e.g. reduced cortical folding), EFs normal to the cortical surface were typically generated (Bindman *et al.* 1964; Purpura & McMurtry, 1965). In this vein, we confirm that *purely* inward currents (normal to the cortical surface) during anodal/cathodal DCS in rat cortical slices result in facilitation/inhibition of synaptic efficacy (Figs 3*C* and 4*C*); notably even afferents to the apical dendrites were modulated based on somatic polarization (c.f. Bikson *et al.* 2004). Specifically, polarization along the somatodendritic axis with radial fields modulated cortical synaptic efficacy of orthodromically activated horizontal and vertical afferents, consistent with postsynaptic soma polarization (Figs 3*C* and 4*C*), and in agreement with results in hippocampal slices (Jefferys, 1981; Bikson *et al.* 2004; Kabakov *et al.* 2012).

Importantly, in the human case with cortical current flow with *both* a radial and tangential component, one cannot ignore the tangential component and *a priori* assume modulation simply based on somatic polarization.

Axon terminal polarization mediates modulation of synaptic efficacy by tangential cortical current flow

Our modelling results (Fig. 2) build on previous efforts (Datta *et al.* 2009; Salvador *et al.* 2010) showing that tDCS generates both radial and tangential fields. But surprisingly, quantification on macro- and micro-scales demonstrates tangential fields dominate radial fields (4–12×) even under the electrodes (the nominal stimulation target). Most of the cortex will have both a radial and a *larger* tangential component to the current flow (Fig. 2*B* and *C*). Tangentially oriented fields do not significantly polarize pyramidal neuron somas (Ranck, 1975; Bikson *et al.* 2006; Radman *et al.* 2009). However, tangential EFs are expected to polarize neuronal elements extending parallel to the cortical surface, notably axons and their synaptic terminals, including corticocortical afferents (Basser & Roth, 2000; Bikson *et al.* 2004, 2006).

Generally, the sensitivity of axon terminals to EFs and the role of terminal membrane potential in synaptic function have been recognized for decades (Purpura & McMurtry, 1965; Hause, 1975; Bikson *et al.* 2004, 2006). Though the polarization of axons and their terminals in the cortex is a complex function of neuronal morphology relative to the EF (Figs 1*C* and 5*A*), we show sufficiently long branch terminals approach the polarization expected for semi-infinite axons: $E\lambda\cos\theta$ (Fig. 5*Bc* and *Cc*). If one considers the diversity and density of axonal afferents, it is reasonable to assume that some axons will have morphology and direction leading to optimal ($E\lambda$) terminal polarization – for any direction EF. λ is thus the effective coupling constant for the most sensitive terminals; ∼0.42–0.55 mm for cortical pyramidal axons (Sasaki *et al.* 2012). Cortical and hippocampal pyramidal somas have a typical coupling constant ∼0.12–0.24 mm (Jefferys, 1981; Bikson *et al.* 2004; Deans *et al.* 2007; Radman *et al.* 2009; Frohlich & McCormick, 2010). This *directionless* terminal coupling constant is independent of and two–three times more sensitive than cortical pyramid somas under *optimally oriented* radial EFs (Hause, 1975; Radman *et al.* 2009). Thus, even under purely radial fields, afferent axon terminals will polarize more than pyramid somas. Moreover, during tDCS EFs are dominantly tangential (Fig. 2), which might indicate a further reduction of pyramid soma polarization, but not afferent axon terminals.

The direction of terminal polarization will depend on the orientation (morphology) of the specific afferent pathway relative to the EF (Figs 3*C* and 4*D*). This is especially relevant for the cortex, where different types of excitatory and inhibitory cells form dense anatomical and functional synaptic circuits that establish routes of information transfer. As a result of the symmetrical orientation of the local synaptic pathways in the primary motor cortex, we demonstrate tangential EFs have no average effect on synaptic efficacy despite pathway-specific effects (Fig. 4*D*); importantly, given distinct pathway-specific functions, a negligible average effect does *not* equate to no net effect on information processing. Concomitant radial and tangential field effects *in vivo* should be addressed in future studies. Our results in cortical brain slices are consistent with tangential EFs that produce synaptic terminal hyperpolarization/depolarization leading to facilitation/inhibition of synaptic efficacy (Figs 3*C* and 4*D*). Similar directional sensitivity to EFs oriented along afferent axons is reported in the hippocampus (Bikson *et al.* 2004; Kabakov *et al.* 2012). These results are in agreement with previous findings on the role of synaptic terminal polarization on synaptic strength, as presynaptic hyperpolarization increases presynaptic action potential size and modulates Ca^{2+} current activation and driving force (Hubbard & Willis, 1962*a*; Takeuchi & Takeuchi, 1962; Miledi & Slater, 1966). Accordingly, release is enhanced by terminal hyperpolarization and decreased by terminal depolarization (Bullock & Hagiwara, 1957; Hubbard & Willis, 1962*b*, 1968; Takeuchi & Takeuchi, 1962; Miledi & Slater, 1966; Dudel, 1971).

Conclusion

We developed an overarching framework for modulation of synaptic efficacy by acute DCS based on a simple qualitative model where the changes in synaptic efficacy are determined by somatic and afferent axon polarization (Fig. 3*C*). The results we observed across four pathways for all field orientation and polarities were consistent with this model (Fig. 4*C* and *D*). Synaptic terminals, therefore, should also be considered as an additional target of modulation during DCS, provided the evidence for a presynaptic contribution to DCS effect (Kabakov *et al.* 2012; Marquez-Ruiz *et al.* 2012) and especially given the role of terminals in information processing and plasticity (Malenka & Nicoll, 1999). Indeed, in this last sense the role of somatic *versus* terminal effects can be considered analogous to the long-standing debate over pre- and postsynaptic locus of long-term potentiation and depression of synaptic efficacy. Both will likely prove important as during tDCS cortical regions are exposed to EFs with both radial and tangential components, such that the somatic effects produced by the radial component would be modulated by concurrent afferent-specific terminal effects in an antagonistic or complementary fashion.

The cellular locus of acute DCS-induced excitability changes (e.g. somas, dendrites, synaptic terminals) is fundamental to understanding the mechanisms of tDCS and rationalizing stimulation strategies. While this study establishes the principle of axon terminal effects, alongside somatic effects, as a plausible target of modulation by DCS, it remains to be established where the functional outcomes of DCS (tDCS) originate. For example, this study addressed only the acute synaptic and non-synaptic effects of short-duration DCS, thus we did not expect long-term plastic changes. Additionally, interneuronal/inhibitory effects on synaptic function were excluded in the present study, though actions on terminals indicate a potential for modulation of inhibitory function, even if interneuron somata are not significantly polarized (Radman et. al. 2009). Moreover, brain slices are relatively quiescent compared with the *in situ* case, with no oscillatory activity or stimulation-matched activation – these factors can be further systematically addressed using brain slice techniques (Nagarajan *et al.* 1993; Frohlich & McCormick, 2010; Reato *et al.* 2010). Notwithstanding these important features, understanding the direct modulation of cortical excitatory transmission by acute DCS is a necessary

building block toward a broader mechanistic understanding.

References

Anastassiou CA, Montgomery SM, Barahona M, Buzsaki G & Koch C (2010). The effect of spatially inhomogeneous extracellular electric fields on neurons. *J Neurosci* **30**, 1925–1936.

Andreasen M & Nedergaard S (1996). Dendritic electrogenesis in rat hippocampal CA1 pyramidal neurons: functional aspects of Na^+ and Ca^{2+} currents in apical dendrites. *Hippocampus* **6**, 79–95.

Antal A, Varga ET, Kincses TZ, Nitsche MA & Paulus W (2004). Oscillatory brain activity and transcranial direct current stimulation in humans. *Neuroreport* **15**, 1307–1310.

Arlotti M, Rahman A, Minhas P & Bikson M (2012). Axon terminal polarization induced by weak uniform DC electric fields: a modeling study. *Conf Proc IEEE Eng Med Biol Soc* **2012**, 4575–4578.

Aroniadou VA & Keller A (1993). The patterns and synaptic properties of horizontal intracortical connections in the rat motor cortex. *J Neurophysiol* **70**, 1553–1569.

Aroniadou VA & Keller A (1995). Mechanisms of LTP induction in rat motor cortex in vitro. *Cereb Cortex* **5**, 353–362.

Ascoli GA (2006). Mobilizing the base of neuroscience data: the case of neuronal morphologies. *Nat Rev Neurosci* **7**, 318–324.

Basser PJ & Roth BJ (2000). New currents in electrical stimulation of excitable tissues. *Annu Rev Biomed Eng* **2**, 377–397.

Bikson M, Dmochowski J & Rahman A (2012*a*). The "quasi-uniform" assumption in animal and computational models of non-invasive electrical stimulation. *Brain Stimul*. (Article in Press DOI: 10.1016/j.brs.2012.11.005).

Bikson M, Inoue M, Akiyama H, Deans JK, Fox JE, Miyakawa H & Jefferys JG (2004). Effects of uniform extracellular DC electric fields on excitability in rat hippocampal slices in vitro. *J Physiol* **557**, 175–190.

Bikson M, Radman T & Datta A (2006). Rational modulation of neuronal processing with applied electric fields. *Conference Proceedings: Annual International Conference of the IEEE Engineering in Medicine and Biology Society IEEE Engineering in Medicine and Biology Society Conference* **1**, 1616–1619.

Bikson M, Reato D & Rahman A (2012*b*). Cellular and network effects of transcranial direct current stimulation: insights from animal models and brain slice. In *Transcranial Brain Stimulation*, 1st edn, ed. Miniussi C, Paulus W & Rossini PM, pp. 456. CRC Press, New York.

Bindman LJ, Lippold OC & Redfearn JW (1964). The action of brief polarizing currents on the cerebral cortex of the rat (1) during current flow and (2) in the production of long-lasting after-effects. *J Physiol* **172**, 369–382.

Bullock TH & Hagiwara S (1957). Intracellular recording from the giant synapse of the squid. *J Gen Physiol* **40**, 565–577.

Castro-Alamancos MA, Donoghue JP & Connors BW (1995). Different forms of synaptic plasticity in somatosensory and motor areas of the neocortex. *J Neurosci* **15**, 5324–5333.

Chan CY, Hounsgaard J & Nicholson C (1988). Effects of electric fields on transmembrane potential and excitability of turtle cerebellar Purkinje cells *in vitro*. *J Physiol* **402**, 751–771.

Chan CY & Nicholson C (1986). Modulation by applied electric fields of Purkinje and stellate cell activity in the isolated turtle cerebellum. *J Physiol* **371**, 89–114.

Creutzfeldt OD, Fromm GH & Kapp H (1962). Influence of transcortical d-c currents on cortical neuronal activity. *Exp Neurol* **5**, 436–452.

Datta A, Baker JM, Bikson M & Fridriksson J (2011). Individualized model predicts brain current flow during transcranial direct-current stimulation treatment in responsive stroke patient. *Brain Stimul* **4**, 169–174.

Datta A, Bansal V, Diaz J, Patel J, Reato D & Bikson M (2009). Gyri-precise head model of transcranial direct current stimulation: improved spatial focality using a ring electrode versus conventional rectangular pad. *Brain Stimul* **2**, 201–207.

Datta A, Truong D, Minhas P, Parra LC & Bikson M (2012). Inter-individual variation during transcranial direct current stimulation and normalization of dose using MRI-derived computational nodels. *Front Psychiatry* **3**, 91.

Deans JK, Powell AD & Jefferys JG (2007). Sensitivity of coherent oscillations in rat hippocampus to AC electric fields. *J Physiol* **583**, 555–565.

Dudel J (1971). The effect of polarizing current on action potential and transmitter release in crayfish motor nerve terminals. *Pflugers Arch* **324**, 227–248.

Fritsch B, Reis J, Martinowich K, Schambra HM, Ji Y, Cohen LG & Lu B (2010). Direct current stimulation promotes BDNF-dependent synaptic plasticity: potential implications for motor learning. *Neuron* **66**, 198–204.

Frohlich F & McCormick DA (2010). Endogenous electric fields may guide neocortical network activity. *Neuron* **67**, 129–143.

Gartside IB (1968). Mechanisms of sustained increases of firing rate of neurones in the rat cerebral cortex after polarization: reverberating circuits or modification of synaptic conductance? *Nature* **220**, 382–383.

Gluckman BJ, Neel EJ, Netoff TI, Ditto WL, Spano ML & Schiff SJ (1996). Electric field suppression of epileptiform activity in hippocampal slices. *J Neurophysiol* **76**, 4202–4205.

Hause L (1975). *A Mathematical Model for Transmembrane Potentials Secondary to Extracellular Fields in Electroanaesthesia: Biomedical and Biophysical Studies*. Academic Press, New York.

Hess G, Aizenman CD & Donoghue JP (1996). Conditions for the induction of long-term potentiation in layer II/III horizontal connections of the rat motor cortex. *J Neurophysiol* **75**, 1765–1778.

Hess G & Donoghue JP (1994). Long-term potentiation of horizontal connections provides a mechanism to reorganize cortical motor maps. *J Neurophysiol* **71**, 2543–2547.

Hubbard JI & Willis WD (1962*a*). Hyperpolarization of mammalian motor nerve terminals. *J Physiol* **163**, 115–137.

Hubbard JI & Willis WD (1962*b*). Mobilization of transmitter by hyperpolarization. *Nature* **193**, 174–175.

Hubbard JI & Willis WD (1968). The effects of depolarization of motor nerve terminals upon the release of transmitter by nerve impulses. *J Physiol* **194**, 381–405.
Jefferys JGR (1981). Influence of electric fields on the excitability of granule cells in guinea-pig hippocampal slices. *J Physiol* **319**, 143–152.
Joucla S & Yvert B (2009). The "mirror" estimate: an intuitive predictor of membrane polarization during extracellular stimulation. *Biophys J* **96**, 3495–3508.
Kabakov AY, Muller PA, Pascual-Leone A, Jensen FE & Rotenberg A (2012). Contribution of axonal orientation to pathway-dependent modulation of excitatory transmission by direct current stimulation in isolated rat hippocampus. *J Neurophysiol* **107**, 1881–1889.
Keller A (1993). Intrinsic synaptic organization of the motor cortex. *Cereb Cortex* **3**, 430–441.
Malenka RC & Nicoll RA (1999). Long-term potentiation–a decade of progress? *Science* **285**, 1870–1874.
Markram H, Wang Y & Tsodyks M (1998). Differential signaling via the same axon of neocortical pyramidal neurons. *Proc Natl Acad Sci U S A* **95**, 5323–5328.
Marquez-Ruiz J, Leal-Campanario R, Sanchez-Campusano R, Molaee-Ardekani B, Wendling F, Miranda PC, Ruffini G, Gruart A & Delgado-Garcia JM (2012). Transcranial direct-current stimulation modulates synaptic mechanisms involved in associative learning in behaving rabbits. *Proc Natl Acad Sci U S A* **109**, 6710–6715.
Miledi R & Slater CR (1966). The action of calcium on neuronal synapses in the squid. *J Physiol* **184**, 473–498.
Miranda PC, Correia L, Salvador R & Basser PJ (2007). The role of tissue heterogeneity in neural stimulation by applied electric fields. *Conf Proc IEEE Eng Med Biol Soc* **2007**, 1715–1718.
Miranda PC, Lomarev M & Hallett M (2006). Modeling the current distribution during transcranial direct current stimulation. *Clin Neurophysiol* **117**, 1623–1629.
Nagarajan SS, Durand DM & Warman EN (1993). Effects of induced electric fields on finite neuronal structures: a simulation study. *IEEE Trans Biomed Eng* **40**, 1175–1188.
Nitsche MA & Paulus W (2000). Excitability changes induced in the human motor cortex by weak transcranial direct current stimulation. *J Physiol* **527(Pt 3),** 633–639.
Nitsche MA & Paulus W (2001). Sustained excitability elevations induced by transcranial DC motor cortex stimulation in humans. *Neurology* **57**, 1899–1901.
Nitsche MA, Seeber A, Frommann K, Klein CC, Rochford C, Nitsche MS, Fricke K, Liebetanz D, Lang N, Antal A, Paulus W & Tergau F (2005). Modulating parameters of excitability during and after transcranial direct current stimulation of the human motor cortex. *J Physiol* **568**, 291–303.
Purpura DP & McMurtry JG (1965). Intracellular activities and evoked potential changes during polarization of motor cortex. *J Neurophysiol* **28**, 166–185.
Radman T, Ramos RL, Brumberg JC & Bikson M (2009). Role of cortical cell type and morphology in subthreshold and suprathreshold uniform electric field stimulation in vitro. *Brain Stimul* **2**, 215–228.
Ranck JB, Jr (1975). Which elements are excited in electrical stimulation of mammalian central nervous system: a review. *Brain Res* **98**, 417–440.
Ranieri F, Podda MV, Riccardi E, Frisullo G, Dileone M, Profice P, Pilato F, Di Lazzaro V & Grassi C (2012). Modulation of LTP at rat hippocampal Ca3-Ca1 synapses by direct current stimulation. *J Neurophysiol* **107**, 1868–1880.
Reato D, Rahman A, Bikson M & Parra LC (2010). Low-intensity electrical stimulation affects network dynamics by modulating population rate and spike timing. *J Neurosci* **30**, 15067–15079.
Rioult-Pedotti MS, Friedman D, Hess G & Donoghue JP (1998). Strengthening of horizontal cortical connections following skill learning. *Nat Neurosci* **1**, 230–234.
Salvador R, Mekonnen A, Ruffini G & Miranda PC (2010). Modeling the electric field induced in a high resolution realistic head model during transcranial current stimulation. *Conf Proc IEEE Eng Med Biol Soc* **2010**, 2073–2076.
Sasaki T, Matsuki N & Ikegaya Y (2012). Effects of axonal topology on the somatic modulation of synaptic outputs. *J Neurosci* **32**, 2868–2876.
Takeuchi A & Takeuchi N (1962). Electrical changes in pre- and postsynaptic axons of the giant synapse of Loligo. *J Gen Physiol* **45**, 1181–1193.
Terzuolo CA & Bullock TH (1956). Measurement of imposed voltage gradient adequate to modulate neuronal firing. *Proc Natl Acad Sci U S A* **42**, 687–694.
Tranchina D & Nicholson C (1986). A model for the polarization of neurons by extrinsically applied electric fields. *Biophys J* **50**, 1139–1156.
Wang Y, Gupta A, Toledo-Rodriguez M, Wu CZ & Markram H (2002). Anatomical, physiological, molecular and circuit properties of nest basket cells in the developing somatosensory cortex. *Cerebral Cortex* **12**, 395–410.

Author contributions

All experiments and simulations were conducted at the Neural Engineering Laboratory, Department of Biomedical Engineering, The City College of The City University of New York. A.R.: conception and design of the experiments, collection, analysis and interpretation of data, drafting the article, revising it critically for important intellectual content, final approval of the version to be published; D.R.: conception and design of the experiments, interpretation of data, revising it critically for important intellectual content, final approval of the version to be published; A.M.: collection and analysis of data, revising article critically for important intellectual content, final approval of the version to be published; G.F.: collection and analysis of data, revising article critically for important intellectual content, final approval of the version to be published; A.D.: collection and analysis of data, revising article critically for important intellectual content, final approval of the version to be published; L.C.P.: conception and design of the experiments, interpretation of data, revising it critically for

important intellectual content, final approval of the version to be published; M.B.: conception and design of the experiments, interpretation of data, drafting the article, revising it critically for important intellectual content, final approval of the version to be published.

Acknowledgements

This research was supported by National Institutes of Health-National Institute of General Medical Science Grant 41341-03, the Wallace H. Coulter Foundation, and USAF Air Force Research Lab Grant No. FA9550-13-1-0073. The authors declare no competing financial interests.